American Mineralogist, Volume 71, pages 989–998, 1986

Variations in the framework structure of the zeolite ferrierite

Brad K. Smith
Department of Geology, Arizona State University, Tempe, Arizona 85287

Abstract

The possibilities of lower symmetry and composite structures have been explored using transmission electron microscopy for the zeolite ferrierite [ideal composition $Na_2Mg_2Al_6Si_{30}O_{72}\cdot 18(H_2O)$]. The *Immm* symmetry of ferrierite contains bond angles and lengths that are indicative of an average structure, yet the TEM analysis of ferrierites from three localities determined that most crystals show no deviation from *Immm* even for very small sample volumes. For those crystals that do contain reflections forbidden in the orthorhombic structure, several different types of incommensurate and commensurate structures were observed. Typically, these structures appear to involve thin intergrowths or faults along (010), with less common defects on (110) and (100). Crystallographic models have been derived for these faults of two main types: (1) shearing parallel to [001] of $c/2$ or (2) removal or insertion of specific T–O linkages on these planes. Whereas the electron-diffraction data generally do not support the growth of *Cmmm* domains (as opposed to earlier work that found streaking of l odd rows to be much more pronounced than on l even), contrast simulation of high-resolution micrographs is more consistent with the shearing model than the contraction-expansion model. Ordering was less frequently observed, with extra reflections parallel to the $\langle 011\rangle^*$ zones most common. Because of the highly variable ordering schemes found in ferrierite, there appears to be no simple manner by which the defects or intergrowths combine to produce ordered domains. Large domains of perfect *Cmmm* structure are not consistent with the extra reflections that have been found.

Introduction

Ferrierite is a rare zeolite mineral with known occurrences essentially restricted to filled vesicles in altered basalts and andesites (Wise and Tschernich, 1976), although one diagenetic occurrence in tuffaceous sediments is known (Regis, 1970). Based on a unit cell of 72 oxygens, the framework composition varies from $Al_{8.5}Si_{27.5}O_{72}$ to $Al_5Si_{31}O_{72}$, making ferrierite a silica-rich zeolite with parageneses similar to other low-grade alteration products such as mordenite, clinoptilolite, and heulandite. The major cations found in the exchange sites are Na, Mg, K, and Ca, respectively, although there are wide variations in their relative concentrations.

X-ray crystal-structure refinements of ferrierite have generally indicated an *Immm* symmetry for the framework atoms (Vaughan, 1966; Gramlich-Meier et al., 1984) although a monoclinic ferrierite structure has also been determined (Gramlich-Meier et al., 1985). The topology of the *Immm* framework can be described in terms of a 5-1 secondary building unit (Meier, 1968), which is the structural characteristic of the mordenite family zeolites (mordenite, ferrierite, bikitaitie, epistilbite, dachiardite, and several synthetic zeolites). A diagram of the orthorhombic ferrierite structure is shown in Figure 1a, and a skeletal representation of the framework projected parallel to the c axis is shown in Figure 1b. It may be noted from this figure that the four unique T sites in the *Immm* framework are incompatible with Si-Al ordering for typical ferrierite stoichiometries (Si:Al = 5:1), although Si:Al ordering in other 5-1 family zeolites is known (e.g., mordenite). The stretched T(4)–O(5)–T(4′) bond (T–O–T angle of 180°) is also indicative of an average structure, but it must be emphasized that no lower-symmetry deviations from the *Immm* structure have been noted in the X-ray refined structures (except for the one monoclinic example above).

An earlier analysis of selected-area electron-diffraction patterns (SADs) led to the postulate that two different classes of framework defects were consistent with observed departures from *Immm* symmetry (Gramlich-Meier et al., 1984), although no attempt was made in that paper to determine to what extent one class of defect predominates over the other. These two defects were constrained by the diffraction patterns to be (1) planar, (2) generally restricted to the (010) plane, and (3) very thin (less than about 10 unit cells in thickness), as indicated by the continuous streaking of diffraction points on relevant SADs. In summary, the two faults can be described as follows:

Two-dimensional contraction or expansion faults (Fig. 2). These were modeled on the basis of so-called sigma transformations (cf. Shoemaker et al., 1973), whereby planar arrangements of –O–T– chains are either inserted

0003–004X/86/0708–0989$02.00

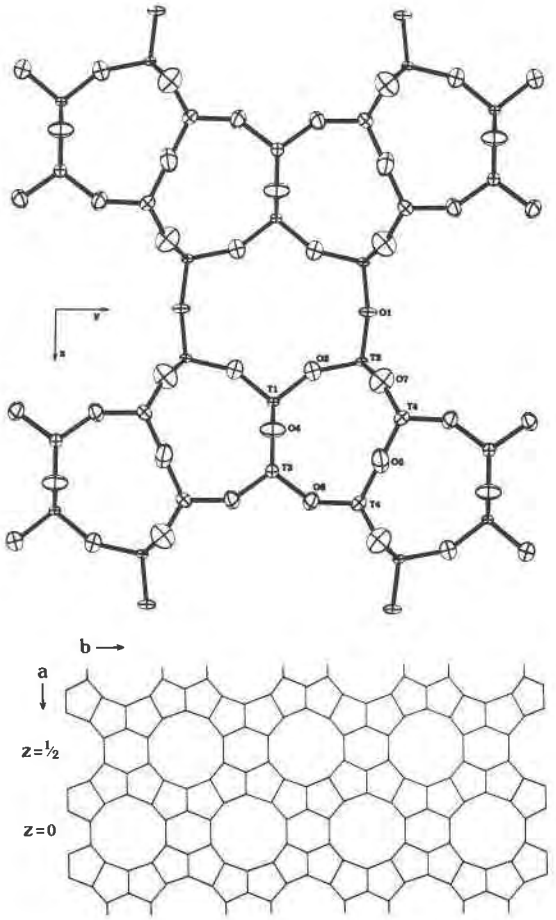

Fig. 1. Crystal structure of *Immm* ferrierite. (a) View down [001] from refinement of Gramlich-Meier et al. (1985). (b) Skeletal framework structure projected down [001] of several unit cells; z in left margin refers to height of six-ring rows.

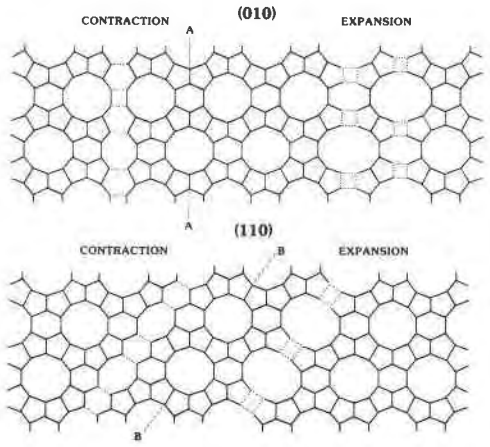

Fig. 2. Schematic crystal structures viewed down [001] for the sigma transformation fault models. Top structures are (010) faults; lower structures are (110) faults. Note that the (010) expansion fault replicates the mordenite structure *in projection only*; substantial rearrangements of the framework must occur to exactly produce mordenite from the (010) expansion fault in ferrierite.

or removed along crystallographic planes that are either mirrors or very nearly so. For ferrierite, this entails expansion of the T(1)–T(3) linkage into a four-member ring of tetrahedra ("expansion faults"), or removal of this linkage to form a four- and eight-rings in place of six- and ten-rings respectively ("contraction faults"). Both of these faults are necessarily nonconservative because they require the addition or removal of tetrahedral subunits to or from specific sites along a plane within the unit cell.

Thin domains of *Cmmm* structure ferrierite (Fig. 3). The *Cmmm* structure can be visualized by considering all of the tetrahedral links between the 5-1 sheets parallel to (100): if these links are coplanar (on $z = 0$), the resultant structure is *Cmmm,* whereas links at alternating heights (i.e., $z = 0$ and $z = ½$) yield the *Immm* structure (Fig. 1b). An alternative description of this structure is possible by considering the (100) sheets as composed of columns of wollastonite chains parallel to c; for *Immm* ferrierite, these chains alternate by a displacement of $c/2$ parallel to [010]. By disrupting this alternating sequence (e.g., by displacing one chain by $c/2$), the local structure loses the c glide and becomes *Cmmm.*

Recent TEM work by Sanders (1985) substantially confirmed the diffraction evidence for faults on (010) and {110} in ferrierite, although only faults of the second type (conservative, shearing faults) were proposed for the fault structure. This paper reports our TEM work that assesses the possible frequency of occurrence of these faults, together with high-resolution micrographs of the ferrierite structure that are believed to contain the second type of defect.

Electron microscopy

Experimental methods

Three different ferrierite samples were chosen for this study and are described with pertinent specimen characteristics in Table 1. Samples were prepared for the TEM by hand-picking clots of grains from the host rock, crushing these clots with two or three downward strokes in a mortar and pestle, and removing any obvious contaminants from the powder. This powder was then suspended in alcohol and pipetted on a Cu grid covered by a holey C film. No pretreatment or subsequent treatment was applied to extend the electron radiation stability of these samples (cf., Bursill et al., 1981) to avoid any possible modifications of the structure that may be introduced by such treatments.

Observations were made on three microscopes. Conventional TEM analyses were conducted on a JEOL 100C operated at 100 kV and on a Phillips EM400 operated at both 100 and 120 kV. High-resolution microscopy (HRTEM) and some diffraction work was conducted on a JEOL 200CX operated at 200kV with a LaB_6 filament and a ±10° top-entry stage. A perceptible increase in the sta-

Table 1. Characteristics of ferrierites used in the study

NAME:	Silver Mountain	Altoona	Lovelock
REFERENCE[1]:	1	1	2
LATTICE PARAMETERS:			
a	19.224	19.05	19.2[2]
b	14.156	14.14	14.2[2]
c	7.500	7.49	7.5[2]
n	1.483 - 1.486	1.474 - 1.478	1.48
D	- -	- -	2.22
CELL CONTENTS: based on 72 Oxygens			
Si	28.99	30.62	30.1
Al	6.93	5.43	5.9
Fe	0.04	- -	- -
Mg	1.99	0.96	0.32
Ca	0.50	0.44	0.52
Ba	0.45	0.06	- -
Sr	0.10	- -	- -
Na	0.18	1.26	1.44
K	0.84	1.05	2.85

NOTES:
1) References: 1. Wise and Tschernich (1976); 2. Regis (1970)
2) Determined from electron diffraction patterns

bility of ferrierite was observed at 200 kV vs. 100 kV, but the limited tilting range of the higher-voltage microscope together with the predominant (100) habit of the crystallites lying on the C film did not allow us to take advantage of the increased stability to sample other crystallographic orientations for a given grain.

Observations

All three specimens displayed remarkably similar characteristics when observed in the TEM, even though they have substantially different compositions and crystal morphologies. No distinction will therefore be made between these samples in the descriptions that follow except for a few isolated and unique features that were restricted to one sample.

A typical lath of ferrierite is shown at moderate resolution in Figure 4. These crystals generally lie on the (100) form, but other orientations in the [001] zone are not uncommon. An important feature of these laths is that while they appear as geometrically perfect single crystals, they are almost invariably composed of irrationally rotated subgrains (Fig. 4b). Moiré fringes are often observed, but no consistent rotation or translation that would relate two subgrains could be determined from the Moiré pattern. However, it is clear from both the diffraction patterns and the Moiré fringes that the displacements relating the subgrains are small. These subgrain displacements are most easily explained as a growth phenomena, not unlike the surface growth steps found in synthetic chabazite at high resolution (Cartlidge et al., 1983). The disruption of the Moiré fringe images is also indicative of faulting or lattice defects within the subgrains, which will be described in greater detail below.

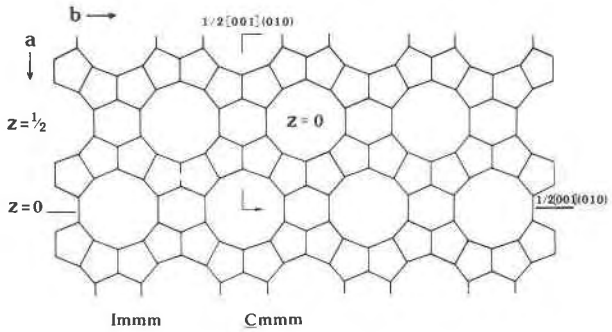

Fig. 3. Schematic framework structures for *Cmmm* domains formed by shears on (010) (top) or (100) (right margin). The structure in projection is identical to that shown in Fig. 1b, with shears translating all six-ring rows to the same height (in this figure, $z = 0$).

Electron diffraction

It must be emphasized that the crystals that showed deviations from *Immmm* symmetry were very rare and infrequently observed. Qualitatively, electron-diffraction effects characteristic of lower symmetries were found in approximately 15–20% of the several hundred grains we

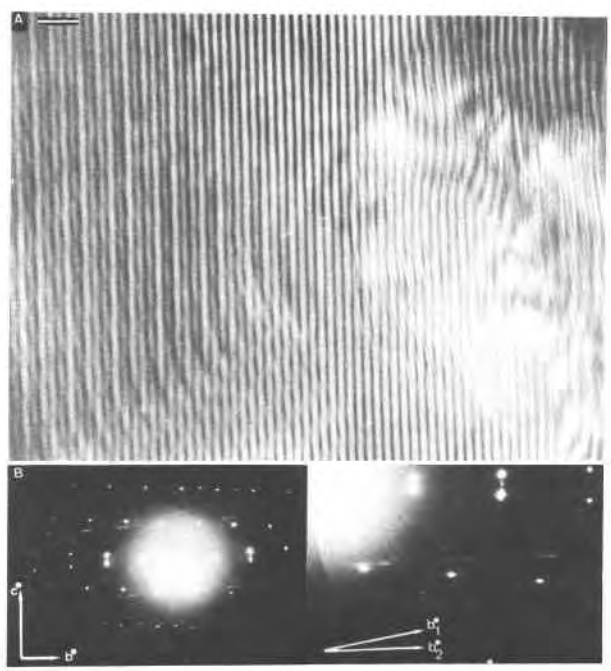

Fig. 4. Growth domains on a single ferrierite crystallite. (a) DF micrograph of domains rotated roughly about [100]. (010) lattice fringes (visible in upper left corner) interfere to produce rotational moiré fringes of 3.0-nm spacing. Scale bar in upper left equals 10.0 nm. Silver Mountain specimen. (b) Rotated SAD of one subgrain containing incommensurate streaks (**b*** streaks parallel to $\mathbf{b}_1$) intergrown with perfect ferrierite subgrain ($\mathbf{b}_2$). Enlargement on right shows the streaking and angular relationship between domains. Silver Mountain.

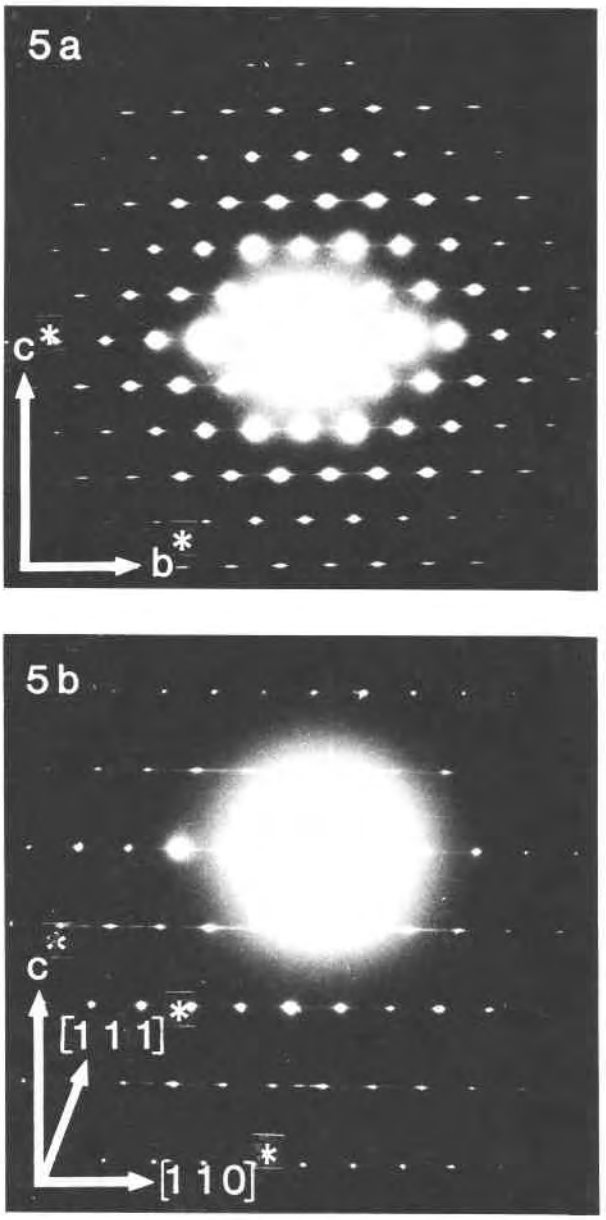

Fig. 5. SADs of incommensurate structures. (a) Continuously streaked reflections superimposed on the *Imm* pattern parallel to **b***. Altoona. (b) [110]* streaks with subsidiary maxima corresponding to roughly ½ [110]*. Streaking is more intense on *l* odd rows. Silver Mountain.

examined. Lack of SAD evidence for lower-symmetry structures overwhelmingly demonstrated that the *Immm* "average structure" is still valid for the smallest possible sample volumes (i.e., using the smallest selected-area apertures). The detection of longer-range modulations was limited both by the experimental conditions listed previously and also by the necessity of using small selected-area apertures to eliminate scattering from neighboring subgrains.

For those grains that did show deviations from *Immm* symmetry in their diffraction patterns, several consistent departures from the *Immm* structure were typically found. These are listed below in order of apparent decreasing prevalence:

Thin (010) intergrowths. These defects were indicated by the presence of elongated or continuously streaked diffraction spikes parallel to the **b*** direction (Fig. 5a). There was no evidence of subsidiary maxima along these streaks (compare with [110]* streaks below), but it was noted that the streak intensity was sometimes greater on *l* odd rows than on *l* even (cf., Gramlich-Meier et al., 1984). However, streaking with different intensity on *l* odd appeared to be much less common than pervasive, consistent intensity streaks on both *l* odd and even. This differs from the observations of Sanders (1985), who reported typically much more intense streaking on *l* odd vs. *l* even rows.

Discontinuous streaking parallel to **b*** also occurs in two typical ways. The first type is a symmetric elongation of the diffraction points, generally occurring in SADs that contain sharp diffraction spots forbidden in *Immm* (Fig. 6a). For these crystals it is likely that the (010) intergrowths responsible for continuously streaked reflections have aligned themselves into a more commensurate structure (as less continuous streaks were commonly accompanied by extra reflections), although it is also possible that the discontinuous streaks also reflect departure of the plane of the intergrowth from exact (010) alignment. In this latter case, the elongation of the reciprocal lattice "rods" (e.g., parallel to [110]*; see below) would not lie exactly in the [100] zone of the diffraction pattern and would terminate symmetrically on either side of the *Immm* diffraction points. Nonsymmetric discontinuous streaks were perhaps more commonly observed, but most of this latter streaking can be attributed to grain-shape factors and secondary diffraction by associated subgrains.

Thin (110) intergrowths. The presence of (110) intergrowths is again indicated by continuous streaks parallel to the [110]* direction in SADs taken down the [1$\bar{1}$0] zone (Fig. 5b). Although streaking indicative of the (110) intergrowths was observed much less commonly than the **b*** streaks, determination of their relative abundance compared to the (010) defect is hampered by the difficulty of obtaining SADs that contain the [110]* direction ([most crystallites lay on the (100) form]. An important feature of the [110]* streaks is the presence of discernible maxima along the streaks at a position of nearly (but not exactly) ½ [110]*. As these maxima do not lie exactly between the [110] row reflections, it is probable that the maxima reflect a long-range, incommensurate ordering of the domains or defects responsible for the continuous [110]* streaks. Tilting experiments by Sanders (1985) also indicated that (110) intergrowths might exist, but no direct observation of [110]* streaks or of subsidiary maxima was reported in that paper.

Other incommensurate intergrowths. Several occurrences of either discontinuous or continuous streaks have been observed parallel to **a*** and ⟨011⟩*, but these seem to be much less common than the two intergrowths men-

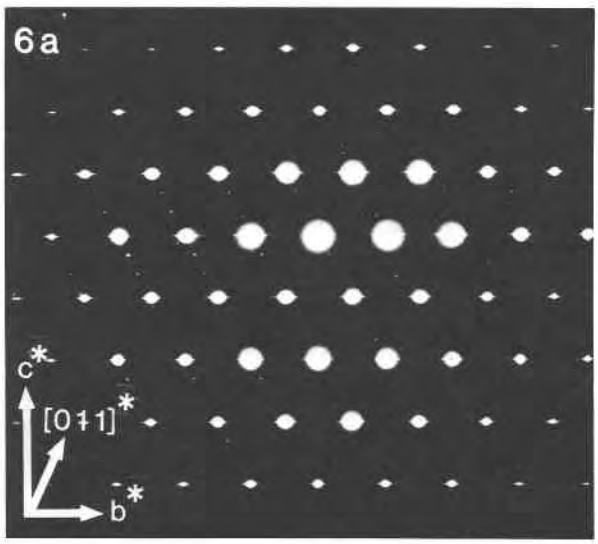

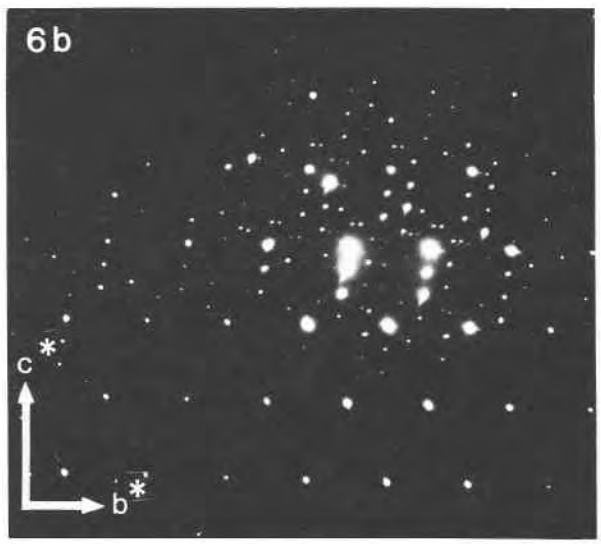

Fig. 6. SADs of ordered structures. (a) Extra reflections and satellitic reflections parallel to [011]*, accompanied with spikes parallel to **b***. Note that extra reflections are aligned parallel to only one ⟨011⟩* direction. Silver Mountain. (b) Incommensurate ordering with satellitic reflections split on the [011] directions. Alignment of extra reflections along **b*** and **c*** is only subparallel to the axes defined by strong reflections of the *Immm* lattice (lower right corner of SAD). Altoona.

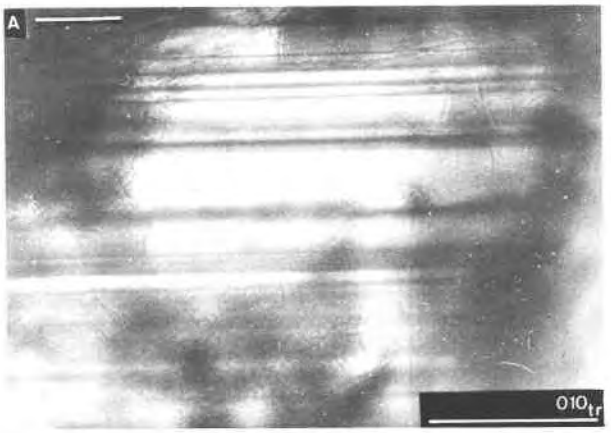

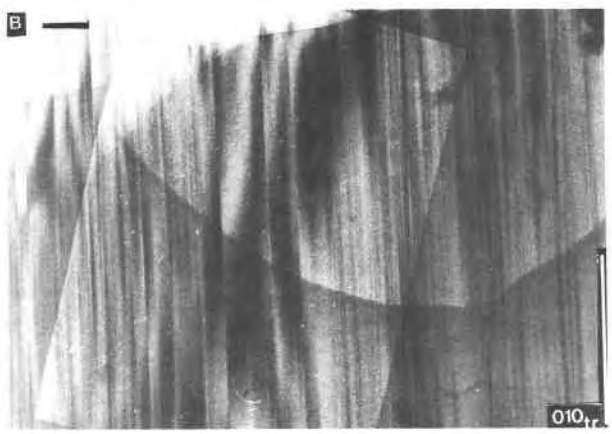

Fig. 7. DF micrographs of lamellar structure along (010). Scale bars in upper left corners are both 0.10 μm in length. (a) Lamellae of roughly 5–30 nm in width. Although the lamellae widths are variable, the interface is restricted to the trace of (010). Altoona. (b) Antiphase boundaries displaying π contrast viewed down approximately [100] with $g = [024]$. Circular feature in right corner is hole in C substrate. Silver Mountain.

tioned above. The ⟨011⟩* streaks are notable in that nearly integral extra reflections are also often aligned in this direction (see below, Fig. 6), but no continuous ⟨011⟩* streaks or other evidence of a very thin (011) intergrowth or domain were found. It is also notable that neither the (100) nor the {011} planes in ferrierite satisfy the relaxed criteria for sigma transformation faults.

Ordered domains. Superlattice reflections were the least common deviation from *Immm* symmetry that was observed in our SADs, and in general there appears to be no obvious relationship between the extra reflections and the thin domain structures described above. Some typical diffraction patterns that contain reflections not attributable to either double diffraction or diffraction from a nearby subgrain are shown in Figure 6. The most common arrays of superlattice points are those aligned parallel to one (of two) ⟨011⟩* directions; these points often occur as a pair of satellites with separations parallel to **b*** and separation distances corresponding to roughly 6.0 nm (i.e., approximately one-fourth $|b^*|$, Fig. 6a). The presence of extra reflections along only one of two equivalent ⟨011⟩ directions is characteristic, even though this streaking may be accompanied by **b*** streaks (Fig. 6a) or extra reflections aligned in other crystallographic directions (Fig. 6b). Superlattice reflections aligned parallel to both ⟨011⟩ directions were never observed. Finally, SAD evidence invariably indicates that the extra reflections are due to an incommensurate ordering of discrete domains (Buseck and Cowley, 1983): spacings of the superlattice reflections with respect to the *Immm* lattice were never integral, and sat-

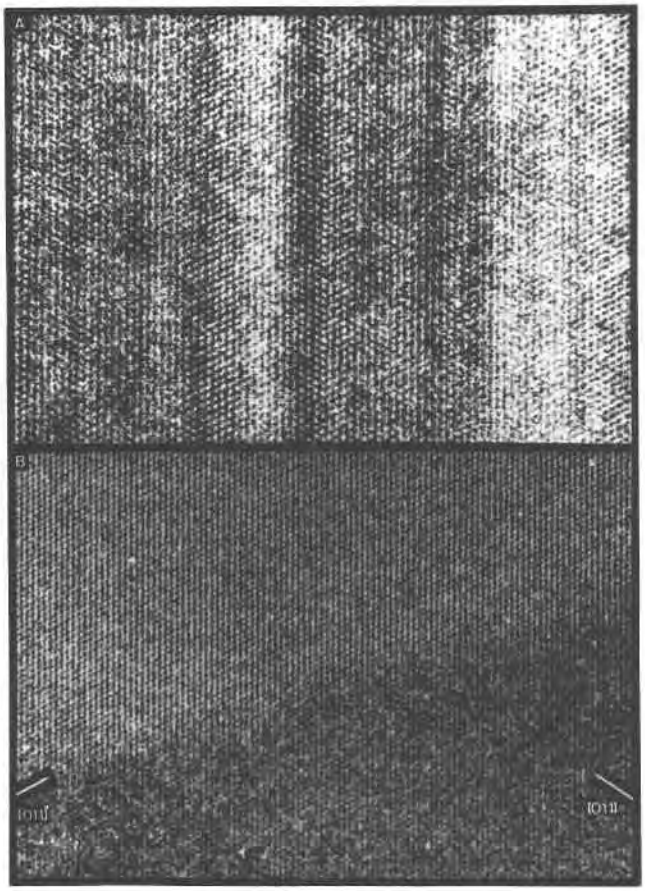

Fig. 8. HRTEM micrographs down [100]. For both micrographs, (010) fringes are the prominent vertical-trending feature. (a) Micrograph used for simulations in Fig. 9. Note that the widths of the fringes are not disturbed across contrast boundaries. Silver Mountain. In (b), only one ⟨011⟩ direction is disturbed ([0$\bar{1}$1]; look down arrows). Also note the change in image across the contrast boundary that trends subparallel to (011) (through center of micrograph).

ellite pairs with several different orientations were common for those crystallites with extra reflections.

Electron imaging

For conventional TEM imaging, we emphasized dark-field (DF) imaging with either streaks or superlattice reflections enclosed in the objective aperture. A typical DF micrograph using an [0k0] streaked reflection is shown in Figure 7a. The lamellae with boundaries parallel to (010) are clearly seen by variations in contrast, and the width of these lamellae (from 5 to about 30 nm) is highly variable. The variation in contrast using a streaked reflection is typically gradational (center of micrograph in Fig. 7a) although some sharp boundaries between the light and dark regions are observed (near top). This contrast variation is attributed to a wide distribution in both (010) domain width and distribution within the ferrierite crystals and indicates that the **b*** streaking contains components due to both very thin domains of a defect structure parallel to (010) (i.e., the thin, sharp changes in contrast) and the distribution of these defects.

For crystals with well-defined superlattice reflections, planar boundaries subparallel with the trace of (010) have also been imaged in DF (Fig. 7b). The asymmetry of the fringe contrast (e.g., near center) is consistent with the diffraction evidence for an incommensurate ordering scheme; symmetric or "π" contrast has not been observed, and ordered structures resulting from displacements that are lattice vectors of *Cmmm* are not plausible. In other words, although we could not uniquely determine the displacement of the fault vectors, the combination of SAD and DF fault contrast preclude the possibility that the lamellae are separate domains of *Cmmm* structure. However, the coincidence of the fault plane and the lamellae interfaces imaged from streaked reflections indicates that the ordering process develops through the long-period modulation of the intergrowths into distinct domains with a very large superlattice.

High-resolution micrographs were taken of Silver Mountain samples, looking down or very close to [100]. This is not an especially good orientation for HRTEM of ferrierite, as no channels are parallel to it, but the predominant (100) habit and the low-angle tilting stage prevented easy sampling of other directions. However, the (010) intergrowths were imaged for two grains that displayed diffraction spots enlongated parallel to **b*** in the [100] orientation (Fig. 8). The alternating dark and light contrast in this figure is a function of the different potential surfaces for different structural modifications of ferrierite rather than the kinematical contrast effects displayed in the DF images (cf., Fig. 7a), but the domain widths and very sharp interfaces between the domains in the HRTEM images agree with the domain features observed in the DF micrographs. For comparison, an image of a crystallite that did not display detectable deviations from *Immm* in electron diffraction is shown in Figure 8b. This image contains the interesting feature that one of the ⟨011⟩ directions is frequently disrupted across (010) (labeled [0$\bar{1}$1], looking down arrow at right) whereas the other ⟨011⟩ direction ([011]) is essentially continuous across the micrograph. The (010) lattice fringes are also continuous throughout this image, including the area where the fringes cross a distinct boundary in contrast (separating the upper light half from the lower, darker half) even though both ⟨011⟩ and the [001] directions are deflected across this feature.

It can be seen in both high-resolution micrographs that the spacing of the (010) lattice fringes remains constant across the image. This is true even in Figure 8a, even though there are pronounced differences in the image of the (010) fringes themselves. The contractions or expansions that are seemingly present in this image therefore express a change in the fringe width or contrast itself, rather than a change in spacing of the fringe.

Table 2. DLS final parameters for fault models

		I	II	III
Model:		(010) Contraction	(110) Contraction	
S.G.:		Pmmn	B2/m	Cmmm
Lattice Constants:				
a		19.22	23.85[1]	19.20
b		11.53	9.43	14.12
c		7.49	7.49	7.49
gamma		-	114.34	-
Atomic Positions:				
T(1)	x	.1558	.0672	.1560
	y	0.0	.2817	0.0
	z	0.0	0.0	0.0
T(2)	x	.0829	.1558	.0830
	y	.2454	.6445	.2004
	z	0.0	0.0	0.0
T(3)	x	.2733	.0753	.2736
	y	0.0	.8444	0.0
	z	.2926	0.0	.2930
T(4)	x	.3223	.1098	.1763
	y	.2501	.1074	.2952
	z	.2072	.2903	.2916
T(5)	x	.1747	.2484	-
	y	.3638	.3321	-
	z	.2927	.2097	-
T(6)	x	.4189	-	-
	y	.3621	-	-
	z	0.5	-	-
O(1)	x	0.0	-.0027	0.0
	y	.2521	.2659	.2061
	z	0.0	0.0	0.0
O(2)	x	.2524	.1132	.2521
	y	0.0	.4619	0.0
	z	0.5	0.0	0.5
O(3)	x	.1074	.1133	.1074
	y	.1129	.7386	.0921
	z	0.0	0.0	0.0
O(4)	x	.2041	.0787	.2044
	y	0.0	.2026	0.0
	z	.1741	.1783	0.5
O(5)	x	.2481	.0918	0.25
	y	.3066	-.0516	0.25
	z	.2471	.1783	.2368
O(6)	x	.1575	.1832	.1621
	y	.3441	.2027	.2782
	z	0.5	.2735	0.5
O(7)	x	.1141	.0922	.1146
	y	.3073	.0844	.2503
	z	.1744	0.5	.1749
O(8)	x	.3187	0.25	.3199
	y	.1137	0.5	.0927
	z	.2499	0.25	.2513
O(9)	x	.3813	.3017	-
	y	.3101	.3118	-
	z	.3264	.3241	-
O(10)	x	0.5	.2576	-
	y	.3288	.3147	-
	z	0.5	0.0	-
O(11)	x	.4110	-	-
	y	0.5	-	-
	z	0.5	-	-
O(12)	x	.1783	-	-
	y	0.5	-	-
	z	.2523	-	-
O(13)	x	.3409	-	-
	y	.2680	-	-
	z	0.0	-	-
R Value[2]		.0032	.0112	.0042

Notes:

1) (110) faults were refined using a unit cell of with a = [110] of Immm structure, c = c of Immm.

2) Refinement procedure used program of Baerlocher et al. (1978).

Discussion

Compatibility of proposed fault structures with HRTEM images

In order to simulate the diffraction patterns and high-resolution micrographs, several alterations of the basic ferrierite *Immm* framework were derived without considering any changes of the nonframework atom positions that would be caused by such framework modifications. For the hypothetical faults outlined in the introduction, these models include (1) a sigma-type contraction on (010) formed by removal of the T(1)–O(4)–T(3) linkage with one pair of the connected O(3),O(8) linkage; (2) faults for the less common defect, a sigma-type contraction on (110), derived by removing the T(4)–O(5)–T(4′) linkage on one of the {110} planes, and (3) *Cmmm* structure—although the models proposed by Gramlich-Meier et al. (1984) involve displacements of the wollastonite chain subunits, the *Cmmm* structure used for this model was derived by shifting the t atoms of the six-ring at ½,½,½ and adjacent T atoms by $c/2$ along the y axis.

The distance least squares ("DLS") method (Baerlocher et al., 1978) was used to generate plausible framework atomic positions for each of these intergrowth models (kindly performed by R. Gramlich-Meier), and the results are listed on Table 2. In terms of the final refinement, no particular intergrowth model was particularly better than another based on the DLS criteria alone.

These structures were then used to simulate the HRTEM images, using operational conditions listed in the caption to Figure 9. The simulation of these images is somewhat subjective, because radiation damage precludes through-focus series and other controls on the imaging conditions which operated when these micrographs were taken. Simulations were performed using both the EMSYS group of programs at the ETH (Skarnulis, 1979) and the multislice–image simulation programs written by Ishizuka (Ishizuka and Uyeda, 1977; Ishizuka, 1980) and maintained at Ar-

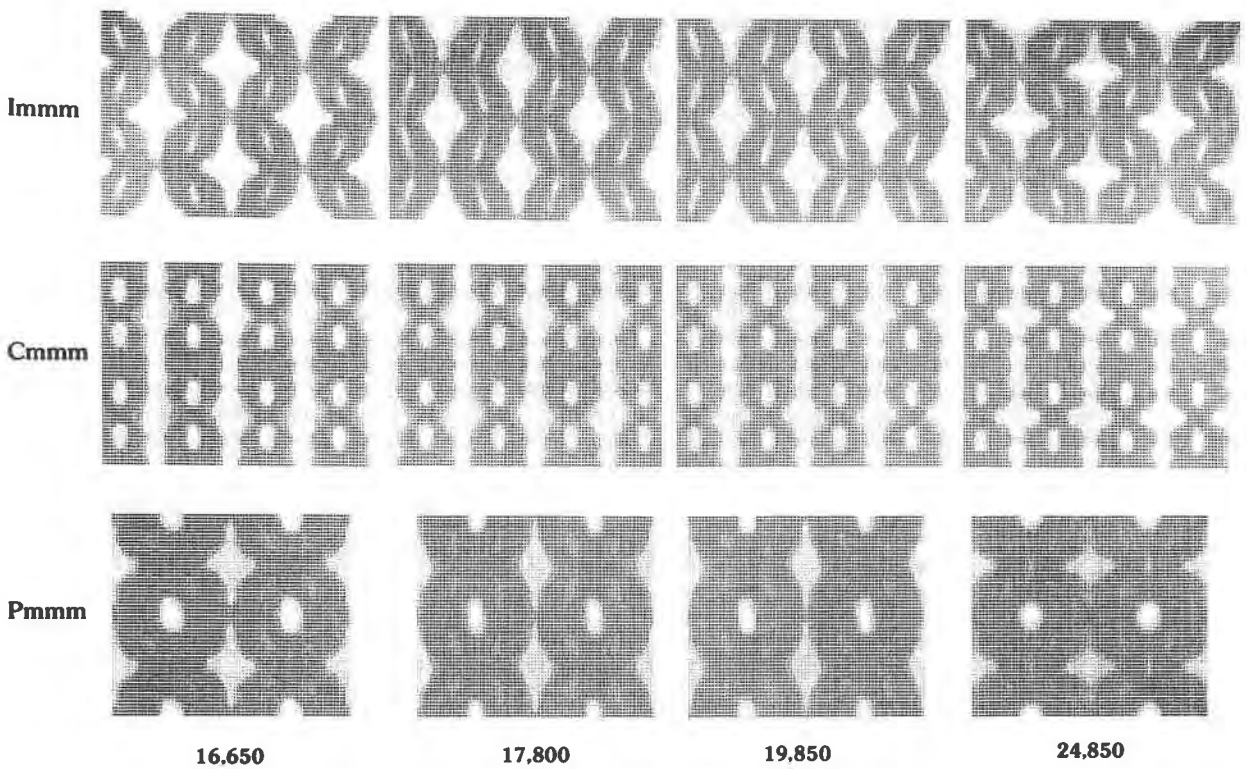

Fig. 9. Image simulations for Fig. 8. Rows correspond to *Immm* structure from Fig. 1, *Cmmm* structure (model III in Table 2), and *Pmmm* contraction fault (model I in Table 2). Pairs of numbers are slice number (with thickness of 0.36 nm) and defocus value (in ångströms). Modeling parameters: C_s = 1.2 mm, depth of focus = 5.0 nm, divergence angle = 0.001 rad, aperture radius = 0.68 $Å^{-1}$, 200 kV.

izona State University. The latter programs were used for runs of the faulted crystal structures (with a larger number of atoms per cell than permitted in EMSYS), but no significant differences between the two program results were encountered in simulations made with identical input.

Simulations of a micrograph in the same series as Figure 8a were attempted using an X-ray refined *Immm* structure of a Silver Mountain ferrierite (Gramlich-Meier et al., 1984) to constrain the thickness and defocus values as closely as possible (Fig. 9, top row). Simulations including the nonframework atoms were essentially identical to the framework-only *Immm* runs, and all subsequent simulations included the framework atoms only. Later runs of the ideal *Pmmm* structure corresponding to the (010) contraction fault and a *Cmmm* structure were then made at the same thickness and defocus values. The {110} faults were not modeled, as no evidence was found in the SADs taken with the Figure 8a series of either streaking or relrod elongation in these directions. Large unit-cell simulations were then made of *Immm-Cmmm* and *Immm-Pmmm* faults, where the fault was placed at $y = 0$ in the unit cell of the *Immm* structure, and a primitive cell was generated with *Immm* structure on one half and one of the DLS intergrowth structures on the other (Fig. 10).

The most notable feature of the high-resolution figures is the disintegration of the network "diamond" pattern in this projection across the (010) bands. In the simulations, this is best shown by the contrast effects caused by loss of the body centering in the *Cmmm* models: the fringe pattern in this structure is more like (010)-parallel fringes rather than the diamond mesh. As indicated by the fringes in Figure 8a, this disruption of the diamond pattern may be correlative to the breakdown in the *Immm* mesh near the contrast-band boundaries. Because the DLS refinements of the *Pmmm* structure necessitated a constriction of *b* lattice parameter for a good fit, the contraction faults as modeled here required the (010) fringes to be more closely spaced, and there is no evidence in the micrographs for such a constriction. Finally, the simulations of the *Pmmm–Immm* faults demonstrate that a strong degradation of the fringe contrast may be expected across the fault boundary, and this drastic change in the contrast of the framework mesh pattern may correspond to the pronounced contrast banding. However, the alteration of the diamond pattern to parallel fringes in the *Cmmm* simulations may also account for this change in contrast. In sum, the *Cmmm* fits correspond best to both the preservation of the fringe spacing and the degradation of the diamond mesh.

Relationship of incommensurate structures to ordered ferrierites

It was already noted in the TEM section that the ordering schemes of ferrierite are highly variable, and it seems unlikely that a simple crystallographic model could describe the various types of commensurate structures that

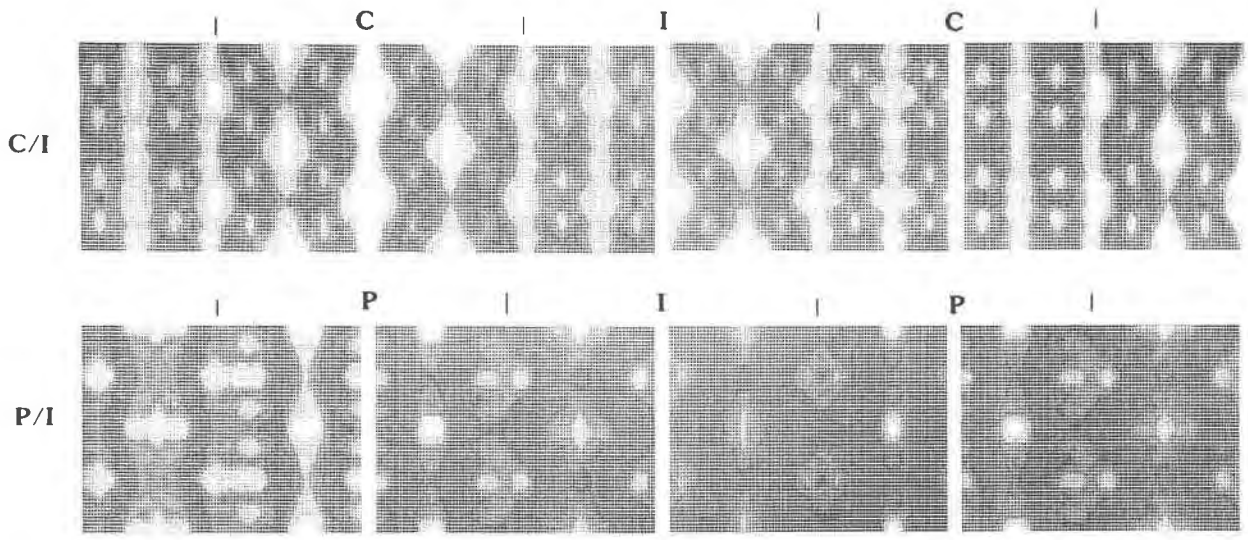

Fig. 10. Image simulations for (010) faults (marked with vertical lines above micrograph). Four columns of images correspond to thickness and defocus values given in Fig. 9.

have been observed. Unlike the incommensurate structures (which are most likely related to shears on specific zones), the sharp extra reflections of the ordered ferrierite are not indicative of any simple crystallographic (much less compositional) modulation.

A possible role of the incommensurate structure in determining the degree of order is consistent with the extra reflections along the ⟨011⟩* directions. From the high-resolution micrographs, the incommensurate structure can be considered as translations (or shears) of columns of six wollastonite chains parallel to [001] on (010) or perhaps {110}. Diffraction evidence and the HRTEM micrographs indicate that these $c/2$[001](010) defects, if terminated within a crystal grain, probably terminate on one specific (011) zone for reasons that are not clear. In other words, domains of the *Cmmm* structure may form by complementary shears of the wollastonite chain columns bounded by two parallel (110) zones. One would then expect that (011) would define the boundaries of different ordered regions rather than (010) (cf. Fig. 7b), but the contrast in this DF image may be explained by stacking-fault contrast due to the partial translation of $c/2$[001](010) rather than antiphase-boundary contrast on (011). Furthermore, before the incommensurate structure may recover into an ordered structure of domains parallel to one (011) zone, the diffraction patterns for the protogrowths should also show much stronger streaking on l odd vs. l even rows, as was observed by Sanders (1985) and occasionally in this study.

Without any consideration of the faulted structures, Al-Si positional order may also be indicated by our diffraction patterns. Of particular interest here are the tetrahedral sheets parallel to (100) composed of the T(3) and T(4) tetrahedra: this sheet is a common topological feature of all mordenite family zeolites (the "puckered six sheet," Meier, 1978). Several crystal structure determinations in the mordenite family have indicated that this six sheet of twenty-four T sites is composed of silica tetrahedra only, which for ferrierite requires that the four T(1) sites and eight T(2) sites would be occupied by the remaining proportion of Si and Al. For stoichiometries in a typical ferrierite range, the remaining sites must be partitioned between four to seven silicons and eight to five aluminums, respectively. Because complete occupation of the T(2) sites by Al contradicts Lowenstein's rule, one is left with some proportion of Al on the T(1) site, and thus the potential for ordering of Al and Si on this site. The T(1) sites define a linkage of the puckered sheets [at O(4)–T(3)] that alternates between pointing inward or outward along the ⟨011⟩ direction, and conceivably chemical partitioning among the T(1) site could be expressed by periodic domains parallel to one or both {011} directions.

The observation of ordering that may be attributed to either accommodation of the shearing defect or positional order on the T(1) and T(2) sites is a new observation in ferrierite, but has analogues in natural zeolites of the mordenite family. It was proposed on the basis of one SAD that ordering parallel to [101]* (structurally analogous to the six-sheet links in the ⟨011⟩* direction in ferrierite) could be possible in a mordenite that displayed reflections forbidden in *Cmcm* (Bursill and Thomas, 1980, their Fig. 4). Stacking polytypism of the six sheets in dachiardite was proposed to explain planar faults observed parallel to (100) on the TEM (Gellens et al., 1982), and although the linkage by four rings in dachiardite is distinctly different from that in ferrierite, these faults support the contention that linking configurations possess inherent flexibility that may permit a variety of structural types.

Role of nonframework atoms in lower-symmetry structures

We have found little evidence for a primary effect of the nonframework species in defining the lower-symmetry structures that we were able to photograph on the TEM.

As noted above, HRTEM simulations and dynamical scattering calculations made as part of these simulations failed to yield significantly different results for models with or excluding nonframework species. However, during the TEM investigation, the presence of a very short lived domain structure (stable for less than 10 s under our illumination conditions) was occasionally noted, and this structure was tentatively attributed to ordering of the nonframework atoms. Given the instability of the structure, we were unable to photograph or otherwise correlate these nonframework domains with the framework intergrowths or faults. It is highly probable that modifications of the channel dimensions parallel to **b** will be induced by the shearing faults on (010) and (110) and that these modifications would certainly be accompanied by localization of the channel species to new locations. The possibility of sigma-type defects, although not as strongly supported by our micrographs as the *Cmmm*-type defect, provides even greater potential for modifying the larger channels parallel to **c**. Given that the defects (of whatever type) are relatively rare, the nonframework domains may indeed bear no relationship to these faults or, in a complementary sense, may induce or stabilize the faulted framework. An interesting observation along this latter point is that synthetic ferrierites studied both by Sanders (1985) and ourselves (Smith, unpub. notes) appear to have much lower densities of defects, which may be attributable to differences in channel species rather than synthesis and/or growth conditions (our natural specimens from widely different environments were remarkably similar).

Conclusions

The defects and ordering described in this paper are exceptional (rather than common) variants of the framework structures of ferrierite. Both X-ray structure analysis and our TEM investigation demonstrate that the orthorhombic structure of ferrierite is an adequate description down to the smallest of sample volumes. If the anomalous bond angles and lengths are due to averaging, the true substructure must exist at the smallest of scales (less than ten unit cells), as was already suspected by Vaughan (1966). Long-range ordering, when found, is not a simple loss of the body center to *C* centering, but must also be attributed in part to combinations of incommensurate domains. Hence, it does not seem likely that a single, lower-symmetry structure will be sufficient to explain an averaging scheme into *Immm*. In addition, the very rare occurrence of the defects implies that the morphology of the channels and their resultant properties will not be much affected by the defects that may be present.

Acknowledgments

A review of an earlier version of this manuscript by J. Michael Bennett was particularly helpful. I am very grateful for the support and encouragement of W. M. Meier throughout this project, and discussions with him and R. Gramlich-Meier, S. Cartlidge, L. McCusker, and G. Spinnler were very illuminating. Electron microscopy was chiefly conducted at the Solid State Physics Laboratory at ETH-Hoenggerberg under H-U. Nissen, and I am indebted to R. Wessicken at that facility for invaluable technical assistance. This work was financially supported by the Swiss National Science Foundation.

References

Baerlocher, C., Hepp, A., and Meier, W.M. (1978) DLS-76: A program for the simulation of crystal structures by geometric refinement. Institute of Crystallography and Petrology, ETH, Zurich, 124 p.

Bursill, L.A., and Thomas, J.M. (1980) Direct imaging of zeolites at near-atomic resolution. In Recent advances in zeolites, 25–30. 5th International Conference on Zeolites, Naples.

Bursill, L.A., Thomas, J.M., and Rao, K.J. (1981) Stability of zeolites under electron irradiation and imaging of heavy cations in silicates. Nature, 289, 157–158.

Buseck, P.R., and Cowley, J.M. (1983) Modulated and intergrowth structures in minerals and electron microscope methods for their study. American Mineralogist, 68, 18–40.

Cartlidge, S., Wessicken, R., and Nissen, H-U. (1983) Electron microscopy study of zeolite ZK-14: A synthetic chabazite. Physics and Chemistry of Minerals, 9, 139–145.

Gellens, L.R., Price, G.D., and Smith, J.V. (1982) The structural relation between svetlorite and dachiardite. Mineralogical Magazine, 45, 157–161.

Gramlich-Meier, R., Meier, W.M., and Smith, B.K. (1984) On faults in the framework structure of the zeolite ferrierite. Zeitschrift für Kristallographie, 169, 201–210.

Gramlich-Meier, R., Gramlich, V., and Meier, W.M. (1985) The crystal structure of the monoclinic variety of ferrierite. American Mineralogist, 70, 619–623.

Ishizuka, K. (1980) Contrast transfer of crystal images in TEM. Ultramicroscopy, 5, 55–65.

Ishizuka, K., and Uyeda, N. (1977) A new theoretical and practical approach to the multislice method. Acta Crystallographia A, 33, 740–749.

Meier, W.M. (1968) Zeolite structures. In Molecular sieves, 10–25. Society of Chemical Industry Special Publication.

——— (1978) Constituent sheets in the zeolite framework of the mordenite group. In L.B. Sand and F.A. Mumpton, Eds. Natural zeolites: Occurrence, properties, uses, 99–103. Pergamon Press, Oxford.

Regis, A.J. (1970) Occurrences of ferrierite in altered pyroclastics in central Nevada. Geological Society of America Abstracts with Programs, 2, 661.

Sanders, J.V. (1985) Crystallographic faulting in the mordenite group zeolites. Zeolites, 5, 81–90.

Shoemaker, D.P., Robson, H.E., and Broussard, L. (1973) The "sigma transformation" interrelating certain known and hypothetical zeolite structures. In Third International Conference on Molecular Sieves, Proceedings 138–143. Zurich.

Skarnulis, A.J. (1979) A system for interactive electron image calculations. Journal of Applied Crystallography, 12, 636–638.

Vaughan, P.A. (1966) The crystal structure of the zeolite ferrierite. Acta Crystallographia, 21, 983–990.

Wise, W.S., and Tschernich, R.W (1976) Chemical composition of ferrierite. American Mineralogist, 61, 60–66.

Manuscript received September 14, 1984
Manuscript accepted March 18, 1986